Journal of Biomedical Optics

BiomedicalOptics.SPIEDigitalLibrary.org

Removing the polarization artifacts in Mueller matrix images recorded with a birefringent gradient-index lens

Jintao Chang
Nan Zeng
Honghui He
Yihong Guo
Hui Ma

SPIE.

Removing the polarization artifacts in Mueller matrix images recorded with a birefringent gradient-index lens

Jintao Chang,[a,b] Nan Zeng,[b] Honghui He,[b] Yihong Guo,[a,b] and Hui Ma[a,b,*]
[a]Tsinghua University, Department of Physics, Beijing 100084, China
[b]Tsinghua University, Graduate School at Shenzhen, Shenzhen Key Laboratory for Minimal Invasive Medical Technologies, Shenzhen 518055, China

Abstract. We obtained backscattering Mueller matrix images on a cancerous tissue sample through a gradient-index (GRIN) lens and observed strong distortion in all the Mueller matrix elements. By measuring the intrinsic polarization properties of the GRIN lens, which is dominated by birefringence following a radial profile, and applying a matrix inversion method to the distorted Mueller matrix, we are able to remove the artifacts because of the birefringent GRIN lens and recover the polarization features of the sample. The results demonstrate the feasibility to take Mueller matrix measurements using GRIN lenses or other optical components with strong birefringence. [DOI: 10.1117/1.JBO.19.9.095001]

Keywords: gradient-index lenses; birefringence; scattering; medical imaging; polarimetry.

Paper 140378R received Jun. 13, 2014; revised manuscript received Aug. 9, 2014; accepted for publication Aug. 15, 2014; published online Sep. 11, 2014.

1 Introduction

Various polarization imaging techniques have been reported in recent years.[1–12] Because the scattered polarized photons carry rich information on the size, shape, and density of the scatterers and the optical properties of both the scatterers and their ambient media,[8–11] the abundant polarization parameters allow more detailed quantitative characterization of the micro- and macrostructure and optical properties of the tissues, and provide new information for medical doctors.[7–9,12] It has been demonstrated in many recent works that polarization imaging is potentially a powerful tool in clinical diagnosis.[9–12] However, polarization imaging can be affected by the polarization properties of the optical components, such as the intrinsic or stress-induced birefringence in endoscopic lenses[13] and the radially symmetric phase retardance in antireflection-coated, molded aspheric glass lenses.[14] Recently, we obtained Mueller matrix images on cancerous tissue samples through a gradient-index (GRIN) lens and observed strong distortion in all the Mueller matrix elements. We have to characterize in detail the polarization properties of such optical components to remove the artifacts for a reliable measurement.

A GRIN lens uses flat surfaces and a parabolic radial refractive index profile [Fig. 1(a)] to guide light with a cosine ray trace [Fig. 1(c)], gaining advantages in terms of size, weight, and flexibility[15–17] for imaging systems such as miniaturized endoscopes.[18–21] However, the fabrication process can introduce an intrinsic birefringence along the radial direction of the GRIN lens rod,[22,23] as shown in Fig. 1(b). The birefringence value is zero at the center of the lens, and its profile is radially symmetric.

There are many works targeted on the Mueller matrix polarimetry with imperfect optical components.[24,25] In this article, we focus on removing the polarization artifacts in Mueller matrix images recorded with a GRIN lens, and we discuss some important points that we need to pay attention to. We characterize the intrinsic polarization property of the GRIN lens by taking its transmission Mueller matrix using a collimated beam and carrying out the Mueller matrix polar decomposition (MMD),[26] and then apply an imaging restoration method based on matrix inversion to eliminate the influence of the birefringent GRIN lens and recover the true polarization properties of the sample. Although the discussions are targeted to a GRIN lens, the conclusions apply, in general, to the Mueller matrix polarimetry using birefringent optical components. The results demonstrate the feasibility of carrying on the Mueller matrix measurements using GRIN lens or other birefringent optical components, and the possibility of the Mueller matrix endoscopy for clinic diagnosis.

2 Experimental Setup and Methods

As shown in Fig. 2(a), the polarization imaging system is a typical setup for Mueller matrix measurements of arbitrary scattering angles. For the backscattering Mueller matrix measurements, the detection arm is rotated by θ [$\sim$130 deg as shown in Fig. 2(a)].

A light beam from a light-emitting diode source is collimated and passes through a band-pass filter (Thorlabs, Newton, New Jersey, Center × Wavelength = 632.8 nm, FWHM = 3 nm). After a linear polarizer (Thorlabs, extinction ratio >5000:1) and a quarter wave plate (Thorlabs, zero-order plate), the beam is set to six polarization states [horizontal linear (H), vertical linear (V), 45 deg linear (P), 135 deg linear (M), right circular (R), and left circular (L)] and then illuminates the sample. The scattered light from the sample is collected by an

*Address all correspondence to: Hui Ma, E-mail: mahui@tsinghua.edu.cn

objective (LISS 5×) or a long-GRIN lens (as marked by the dotted box A) and then passes a quarter wave plate and a polarizer before being detected by the CCD (Q-imaging Retiga Exi, 12-bit). For each incident polarization state (described as Stokes vector S), the same six polarization components of the scattered light (described as Stokes vector S') are detected by the analyzer, giving 36 images corresponding to different combinations of the six incidence and detection polarization states. The Mueller matrix, which transforms the incident polarized light S into the scattered light S' as shown in Eq. (1) and describes the polarization property of the sample, is calculated according to Eq. (2).[27]

$$S' = M * S, \tag{1}$$

$$M = \begin{bmatrix} m_{11} & m_{12} & m_{13} & m_{14} \\ m_{21} & m_{22} & m_{23} & m_{24} \\ m_{31} & m_{32} & m_{33} & m_{34} \\ m_{41} & m_{42} & m_{43} & m_{44} \end{bmatrix} = \frac{1}{2} \begin{bmatrix} \mathrm{HH}+\mathrm{HV}+\mathrm{VH}+\mathrm{VV} & \mathrm{HH}+\mathrm{HV}-\mathrm{VH}-\mathrm{VV} & \mathrm{PH}+\mathrm{PV}-\mathrm{MP}-\mathrm{MM} & \mathrm{RH}+\mathrm{RV}-\mathrm{LH}-\mathrm{LV} \\ \mathrm{HH}-\mathrm{HV}+\mathrm{VH}-\mathrm{VV} & \mathrm{HH}-\mathrm{HV}-\mathrm{VH}+\mathrm{VV} & \mathrm{PH}-\mathrm{PV}-\mathrm{MH}+\mathrm{MV} & \mathrm{RH}-\mathrm{RV}-\mathrm{LH}+\mathrm{LV} \\ \mathrm{HP}-\mathrm{HM}+\mathrm{VP}-\mathrm{VM} & \mathrm{HP}-\mathrm{HM}-\mathrm{VP}+\mathrm{VM} & \mathrm{PP}-\mathrm{PM}-\mathrm{MP}+\mathrm{MM} & \mathrm{RP}-\mathrm{RM}-\mathrm{LP}+\mathrm{LM} \\ \mathrm{HR}-\mathrm{LL}+\mathrm{VR}-\mathrm{RL} & \mathrm{HR}-\mathrm{VR}+\mathrm{VL}-\mathrm{HL} & \mathrm{PR}-\mathrm{MR}+\mathrm{ML}-\mathrm{PL} & \mathrm{RR}-\mathrm{RL}-\mathrm{LR}+\mathrm{LL} \end{bmatrix}. \tag{2}$$

Here each image is indexed by two capital letters: the first letter represents the incidence polarization state and the second letter represents the detection polarization state.[27]

To examine the influence of the GRIN lens, we switch the imaging system between GRIN-lens and normal-lens modes by placing a GRIN lens or an objective [NA = 0.12, as marked by the dotted box A in Fig. 2(a)] in the optical path to collect the scattered light. The imaging resolutions of the GRIN-lens and normal-lens imaging systems are limited by the optical systems and the pixel size of the CCD. Measured with a USAF1951 resolution target, they are ~11 and 8 μm, respectively. The working distances for the normal-lens mode and the GRIN-lens mode are ~25 and 5 mm, respectively. In this experiment, the transformation from the incident Stokes vector S to the detected Stokes vector S' is determined by the polarization properties of the sample and the imaging lens A. Concerning the possible influence of the imaging lens A on the Mueller matrix images, we can study the inherent polarization properties of the imaging lens A. Experiments have shown that the influences of the objective and the other normal lens assembly are negligible. However, the influence of the GRIN lens is significant. The GRIN lens comes from the imaging module of an endoscope (FEMTO TECHNOLOGY CO. LTD, Xi'an, China). All the experimental results in this article are obtained using the GRIN lens with 60 mm length, 2 mm diameter, and 0.17 NA [marked by a red frame in Fig. 2(c)]. Other GRIN lenses in Fig. 2(c) are also tested and give similar results.

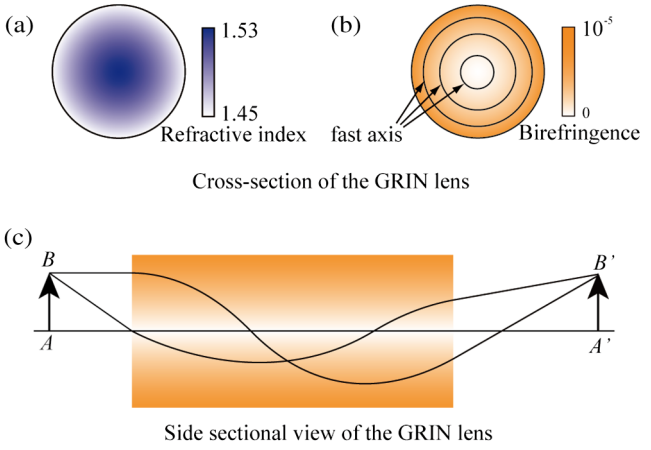

Fig. 1 (a) Schematic diagram of the refractive index distribution on the cross-section of the gradient-index (GRIN) lens. (b) Schematic diagram of the birefringence value and fast axis direction distribution on the cross-section of GRIN lens. (c) Schematic imaging diagram of a GRIN lens. AB is the object and $A'B'$ is the image.

The cancerous tissue sample shown in Fig. 3(a) is a 4-μm-thick paraffin slice of hematoxylin-eosin (HE) stained human skin basal cell carcinoma provided by Shenzhen Sixth People's (Nanshan) Hospital. In Fig. 3(a), the stained colors of the dysplastic region are darker than that of the healthy tissues. Pathological diagnosis identified that the dysplastic region is the basal cell carcinoma tissue. Figure 3(b) shows the unstained 28-μm-thick paraffin slice from the same biopsy sample archived in the hospital. Cancerous areas in Fig. 3(a) are marked with a dashed frame. Because the two slices in Figs. 3(a) and 3(b) are originally twins adjacent to each other, the cancerous areas should look very similar.

3 Experiment Results and Mueller Matrix Restoration

3.1 *Mueller Matrix Imaging of the Sample Measured with the Normal Lens*

We first measure the Mueller matrix of the unstained slice sample using a normal microscope objective lens. This normal-lens system has been calibrated against standard polarization optics, such as quarter and half wave plates, to prove the reliability of the Mueller matrix measurements of the sample. We use oblique illumination and take the backward scattering Mueller matrix of the cancerous tissue sample using the normal-lens mode described in Sec. 2. As shown in Fig. 3(c), many Mueller matrix elements display the clear margin between the normal and the cancerous regions, which is also visible in the wide-field transmission imaging for the HE stained sample [Fig. 3(a)] but not for the unstained sample [Fig. 3(b)]. For comparison, the cancer

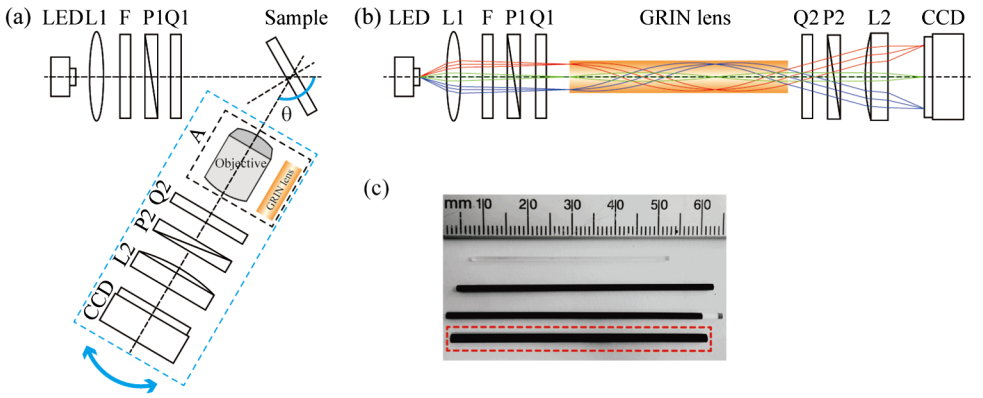

Fig. 2 (a) Schematic diagram of a typical setup for Mueller matrix measurements of arbitrary scattering angles using a normal objective or a GRIN lens. The detection arm A-Q2-P2-L2-CCD can rotate around the sample to measure Mueller matrix in arbitrary angles. (b) Optical layout of the Mueller matrix measurement of the GRIN lens. Birefringence value increases along the radial direction. In this work, the NA of the GRIN lens is small and the incident rays are nearly parallel. L1, the collimating lenses; L2, the imaging lens; F, a band-pass filter; P1 and P2, polarizers; Q1 and Q2, quarter wave plates. (c) Pictures of some tested GRIN lenses, and the experiment results in this article are obtained using a GRIN lens marked by a red dashed frame.

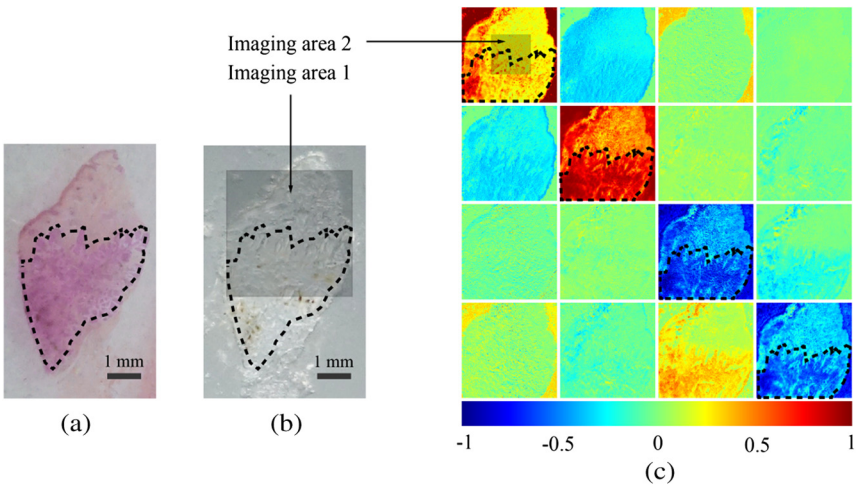

Fig. 3 (a) The hematoxylin-eosin stained slice of basal cell carcinoma of human skin; the dashed lines mark the cancer region. (b) Unstained slice from the same biopsy sample. (c) Mueller matrix image of the unstained slice of the basal cell carcinoma; all the matrix elements are shown in normalized form, with all its elements (except m_{11}) divided by m_{11}. The imaging area of (c) is imaging area 1 shown in (b). The imaging area 2 shown in (c) is the imaging area of the GRIN lens. For comparison, the cancer region in (a) is marked both in (b) and (c).

region in Fig. 3(a) is marked with dashed lines both in Figs. 3(b) and 3(c) and in Figs. 4(a), 4(b), and 4(c). In Fig. 3(c), the region derived from the Mueller matrix agrees roughly with the marked region derived from Fig. 3(a). It should be noted that although the HE stained slice and the unstained slice are adjacent to each other, the cancer regions should look similar but not exactly the same. Thus, it is acceptable if there are some differences between the region derived from the Mueller matrix shown in Fig. 3(c) and the marked region derived from Fig. 3(a).

3.2 *Mueller Matrix of the Sample Measured with the GRIN Lens*

We replace the objective with the GRIN lens and take Mueller matrix images of the same sample. Because of the difference in magnification, the GRIN lens images a smaller area than the objective lens, which is marked as the imaging area 2 in Fig. 3(c). Comparing the undistorted Mueller matrix images [Fig. 4(a)] taken by the normal objective lens with the images taken by the GRIN lens [Fig. 4(b)], it is clear that the GRIN lens distorts the Mueller matrix images seriously, resulting in difficulties in distinguishing the polarization features of the sample. One has to obtain detailed characteristic polarization information of the GRIN lens in order to remove such polarization artifacts.

We can remove the sample and rotate the detection arm of the experimental setup from backscattering to transmission configuration to measure the Mueller matrix of the GRIN lens, shown in Fig. 4(d). For a better description of polarization properties of GRIN lens, we use MMD to quantitatively characterize three basic polarization-sensitive physical processes: diattenuation, phase retardation, and depolarization. As shown in Fig. 5, the polarization property of the GRIN lens is dominated by retardance, which is caused by the linear birefringence of the GRIN

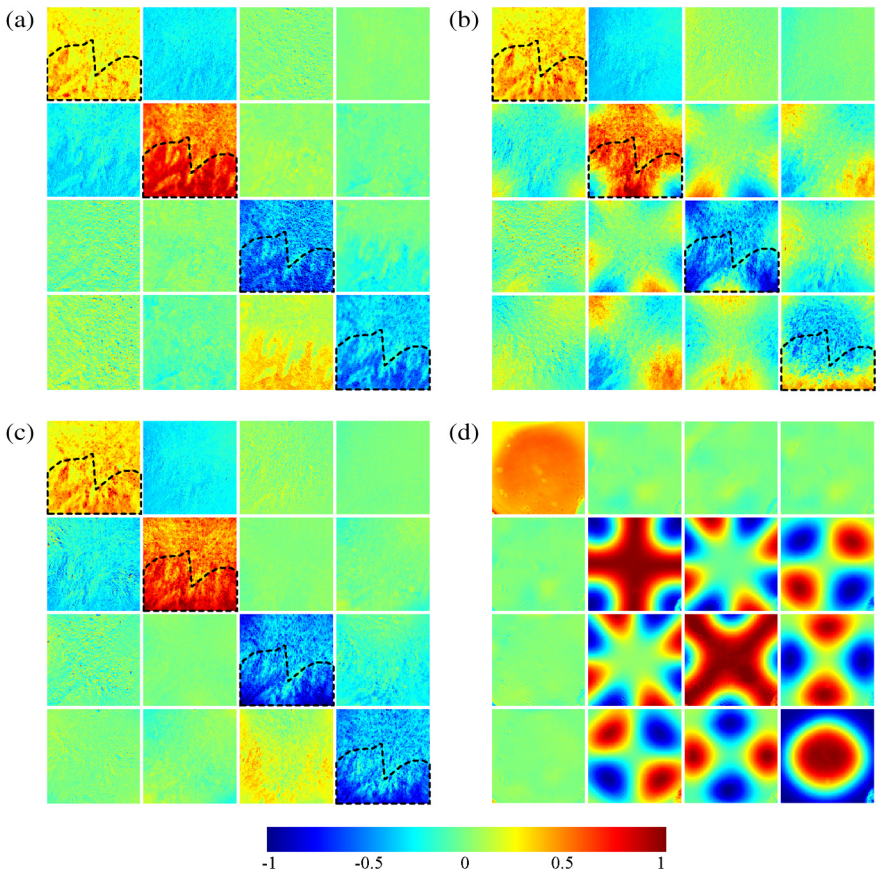

Fig. 4 Mueller matrix images of the sample corresponding to the center part of the images marked by "imaging area 2" in Fig. 3(c), (a) measured through a normal lens objective, (b) measured through a GRIN lens, (c) restored from (b), and (d) Mueller matrix images of the GRIN lens. All the matrixes are shown in normalized form, with all its elements (except m_{11}) divided by m_{11}.

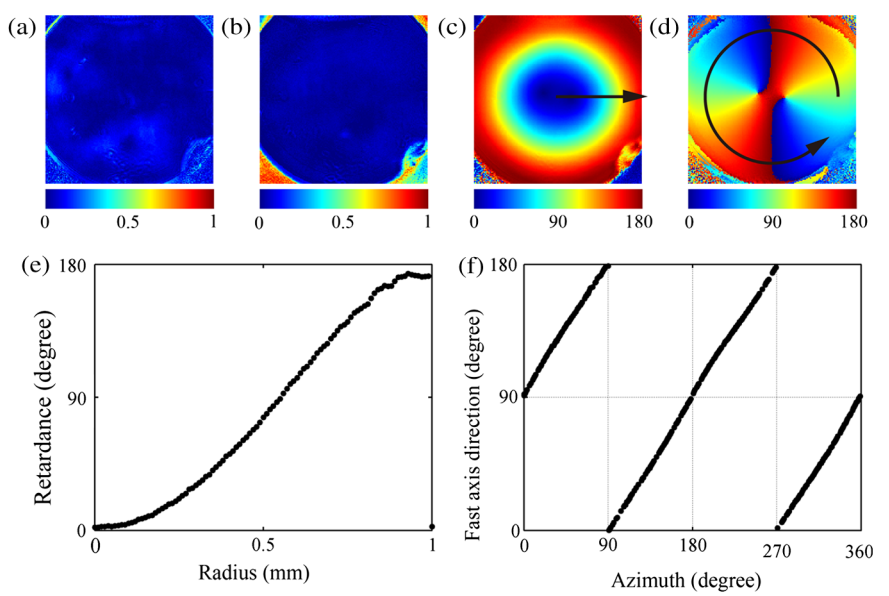

Fig. 5 Mueller matrix decomposition for the GRIN lens: (a) diattenuation, (b) depolarization, (c) linear retardance, (d) fast axis direction, (e) line profile of the linear retardance values along the radius shown in (c), and (f) the line profile of the fast axis directions along the azimuth shown in (d).

lens. Contributions due to both diattenuation and depolarization (partly from stains, surface defects, or other imperfections of the GRIN lens) are small. Figure 5 also shows that the distribution of the linear retardance is approximately radial. It should be noted that both the value of linear retardance and the angle of its fast axis are not strictly radially symmetrical. Such deviation can be attributed to the external force applied to fix the GRIN lens to the assembly. The small abnormal area in the bottom right corner in Figs. 4(d) and 5 corresponds to a defect on the GRIN lens.

In addition, it is worth mentioning that the Mueller matrix of an optical element is related to the incident light angle. The optical layout of the Mueller matrix measurement of the GRIN lens is shown in Fig. 2(b). During the experiments, we have found that the Mueller matrix of the GRIN lens varies slightly with its relative orientation to the incident beam. Such influence can cause a position shift and distortion. For example, the cross-stripe of the Mueller matrix element m22 in Fig. 4(d) would be off center and reshapes smoothly into another asymmetrical stripe. Here the NA of the GRIN lens we used is 0.17; the acceptance angle is so small that the above distortion can be ignored.

3.3 *Mueller Matrix Restoration*

From the above results and analysis, it is obvious that Mueller matrix imaging (MMI) using a GRIN lens cannot be successfully adopted until a proper procedure is developed to correct the polarization effects due to the GRIN lens. In theory, the Mueller matrix M of a component can be eliminated by introducing its inverse matrix, because $\mathrm{inv}(M) * M = I$, where $\mathrm{inv}(M)$ means the inverse of the matrix M and I is the identity matrix, provided that the experimental error is small enough and the matrix M is nonsingular. Thus, if we can measure the Mueller matrix of the GRIN lens M_1, and the combined Mueller matrix of the sample and the GRIN lens M_2, which includes the contributions from the Mueller matrices of the sample, M_3, and the GRIN lens, $M_1{}'$, we can recover the Mueller matrix of the sample M_3 using the following relations:

$$M_2 = M_1{}' * M_3, \tag{3}$$

$$M_3 = \mathrm{inv}(M_1{}') * M_2, \tag{4}$$

where $\mathrm{inv}(M_1{}')$ means the inverse of the matrix $M_1{}'$.

The necessary condition of using Eqs. (3) and (4) is that

$$M_1{}' = M_1. \tag{5}$$

Equation (5) means that we need $M_1{}'$ rather than M_1 to eliminate the artifacts from the GRIN lens. Note that although both M_1 and $M_1{}'$ represent the Mueller matrices of the GRIN lens, they are not necessarily the same. As mentioned in the end of Sec. 3.2, we have noted that the Mueller matrix of the GRIN lens changes with the angular distribution of the incident light, so that beams of different incident angles sample different subsets of the angle-dependent Mueller matrix. When we measure M_1, we use a collimated incident beam parallel to the optical axis of the GRIN lens. When we measure M_2, however, the backscattered light follows a different angular distribution and may sample a different Mueller matrix $M_1{}'$. In the current experiments, the GRIN lens of small NA acts as a spatial filter collecting only those backscattered photons nearly parallel to GRIN lens optical axis. In this case, Eq. (5) is approximately satisfied.

Figure 4(c) shows the restored Mueller matrix images, which are calculated from the experimental results of Figs. 4(b) and 4(d) according to Eq. (4). Compared with undistorted Mueller matrix images as shown in Fig. 4(b), the restoration process recovers the polarization features of the sample from the experimental results seriously distorted by the birefringent GRIN lens.

In order to see the differences of Mueller matrices in Fig. 4 more clearly, we redraw the elements m_{22}, m_{33}, and m_{44} from Figs. 4(a), 4(b), and 4(c) with a different color map, shown in Figs. 6(a1), 6(b1), and 6(c1), respectively. To quantitatively assess the effectiveness of the above restoration process, we extract three rows of data from Mueller matrix images, as shown in Figs. 6(a1), 6(b1), and 6(c1) by the horizontal red lines, and plot the values of the Mueller matrix elements m_{22}, m_{33}, and m_{44} along the selected rows as shown in Figs. 6(a2), 6(b2), and 6(c2), respectively. In order to clearly show how the restoration works, we choose the lines far away from the center where the distortions are more serious. The mean deviations of the distorted (red lines) and the original (dark lines) m_{22}, m_{33}, and m_{44} are 0.61, 0.41, and 0.90, respectively. And the mean deviations of the recovered (blue lines) and the original m_{22}, m_{33}, and m_{44} are 0.08, 0.08, and 0.06, respectively. Apparently, there are significant differences between the distorted and the original m_{22}, m_{33}, and m_{44}, but the differences between the recovered and the original Mueller matrix elements are much smaller. Such a good agreement validates the effectiveness of the restoration technique by the matrix inversion. Some minor errors remaining in the restoration are mainly because of the different optical aberrations between the objective and the GRIN lens across the field of view. In addition, Fig. 4(a) comes from just one direct measurement, but Fig. 4(c) is based on two experiments and the matrix calculation, which may introduce extra errors.

4 Discussions

We have demonstrated that the image restoration technique works for a birefringent GRIN lens. In fact, this technique can also be applied to remove the polarization artifacts from other types of polarization optical components, as long as birefringence is the dominant polarization effect. There are other concerns before using a GRIN lens for Mueller matrix measurements.

Mathematically, if the determinant of the Mueller matrix for an optical component is zero, we cannot obtain the inverse matrix and the restoration technique fails. In experiments, the determinant of a measured Mueller matrix is less likely to reach zero but can be close to it because of the inevitable scattering of the stains and the reflection from the lens surfaces in the optical trains. We can use a condition number of a matrix as an indicator to estimate whether the inversion operation is suitable for the Mueller matrix of an optical component. The condition number has been used to assess the response of a system described by a matrix to the input error in many applications.[28] When the condition number is close to one, an inverse matrix can be computed with good accuracy. For a linear polarizer or a depolarizer, one cannot recover the original polarization characteristics. A detailed analysis on this issue is beyond the scope of this discussion and will be presented in another article. In general, with the increasing diattenuation and depolarization effects,

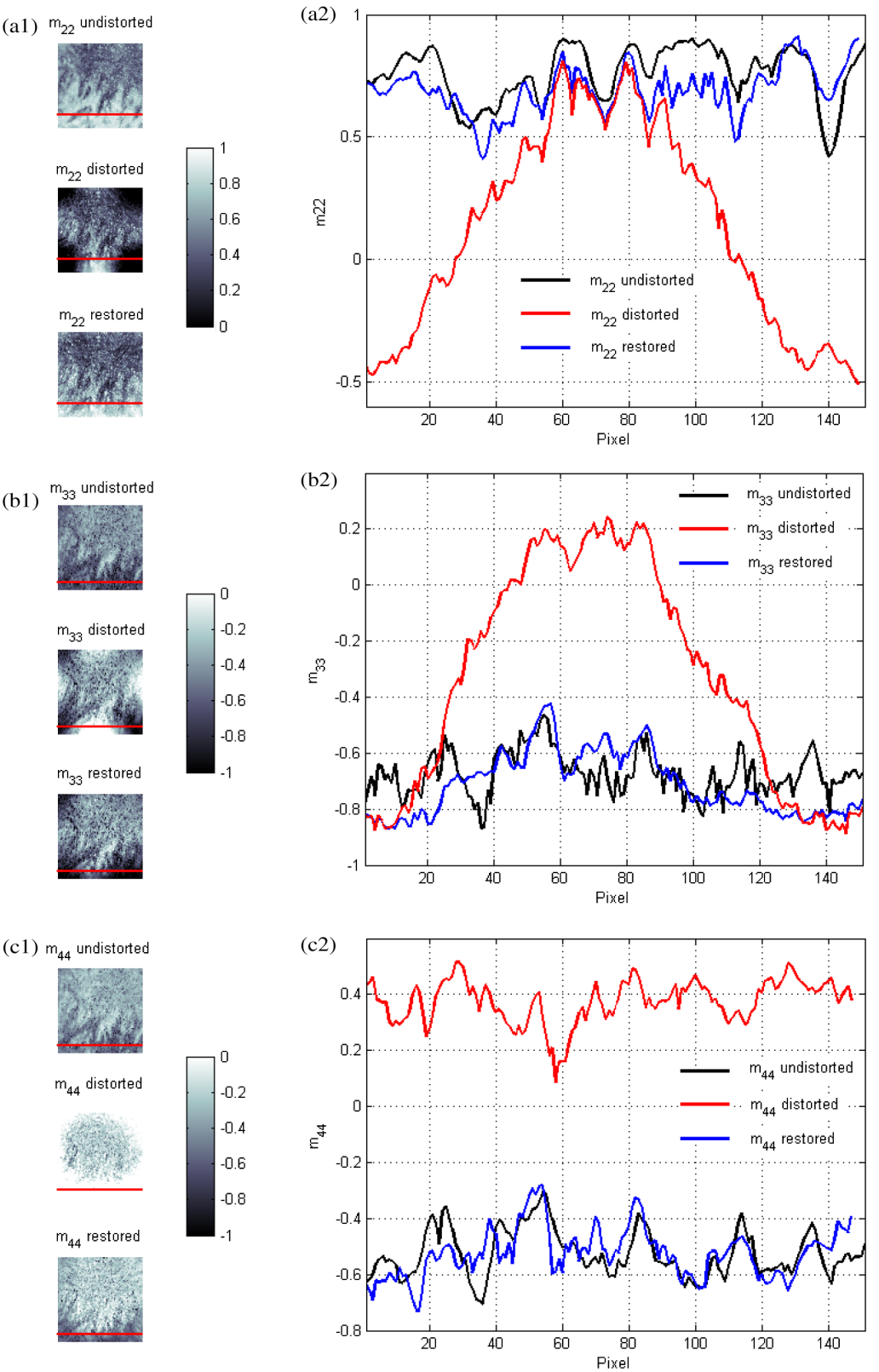

Fig. 6 (a1), (b1), and (c1) The undistorted, distorted, and restored images of m_{22}, m_{33}, and m_{44}, respectively. (a2), (b2), and (c2) Comparison of the undistorted, distorted, and restored images of m_{22}, m_{33}, and m_{44} along the selected rows of data marked by the red lines.

the condition number of a Mueller matrix increases and the uncertainty of matrix inversion increases, too. Fortunately, for many optics components, such as normal imaging lenses, diattenuation and depolarization are usually very small, and the matrix restoration method described here can be applied.

We use the approximation $M_1' = M_1$ for the matrix inversion. By ray tracing, it can be deduced that the optical linear retardation is approximately inversely proportional to the direction cosine of the light ray with respect to the axis. For the GRIN lens used in our research work, the small NA of 0.17 allows only a limited divergence angle for the backscattered photons to pass through, which causes small deviation in the observed retardance of the GRIN lens. So it is rational to use the approximation $M_1' = M_1$ when the NA of the GRIN lens is small.

5 Conclusions

We have performed backscattering Mueller matrix measurements on a cancerous tissue sample using a birefringent GRIN lens. The Mueller matrix images are seriously distorted by the GRIN lens whose polarization properties are dominated by a radial distribution of the birefringence. We used an image restoration method based on matrix operations. By taking the Mueller matrix images of the GRIN lens and calculating its inversion, we can remove the artifacts from the GRIN lens from the distorted images and recover all the polarization features of the sample. This method works well as long as birefringence is the dominant effect of the GRIN lens and NA is relatively small. The results demonstrate the feasibility of carrying on Mueller matrix measurements using birefringent optical components.

Acknowledgments

This work has been supported by National Natural Science Foundation of China Grant Nos. 11174178, 11374179, and 61205199.

References

1. S. L. Jacques, J. C. R. Roman, and K. Lee, "Imaging skin pathology with polarized light," *J. Biomed. Opt.* **7**(3), 329–340 (2002).
2. J. C. Ramella-Roman et al., "Design, testing, and clinical studies of a handheld polarized light camera," *J. Biomed. Opt.* **9**(6), 1305–1310 (2004).
3. L. Qiu et al., "Multispectral scanning during endoscopy guides biopsy of dysplasia in Barrett's esophagus," *Nat. Med.* **16**(5), 603–606 (2010).
4. P. Shukla and A. Pradhan, "Mueller decomposition images for cervical tissue: potential for discriminating normal and dysplastic states," *Opt. Express* **17**(3), 1600–1609 (2009).
5. M. R. Antonelli et al., "Impact of model parameters on Monte Carlo simulations of backscattering Mueller matrix images of colon tissue," *Biomed. Opt. Express* **2**(7), 1836–1851 (2011).
6. R. S. Gurjar et al., "Imaging human epithelial properties with polarized light-scattering spectroscopy," *Nat. Med.* **7**(11), 1245–1248 (2001).
7. N. Ghosh and I. A. Vitkin, "Tissue polarimetry: concepts, challenges, applications, and outlook," *J. Biomed. Opt.* **16**(11), 110801 (2011).
8. H. He et al., "A possible quantitative Mueller matrix transformation technique for anisotropic scattering media," *Photon. Lasers Med.* **2**(2), 129–137 (2013).
9. A. Pierangelo et al., "*Ex-vivo* characterization of human colon cancer by Mueller polarimetric imaging," *Opt. Express* **19**(2), 1582–1593 (2011).
10. A. Pierangelo et al., "Polarimetric imaging of uterine cervix: a case study," *Opt. Express* **21**(12), 14120–14130 (2013).
11. T. Novikova et al., "The origins of polarimetric image contrast between healthy and cancerous human colon tissue," *Appl. Phys. Lett.* **102**(24), 241103 (2013).
12. E. Du et al., "Mueller polarimetry for the detection of cancers," *Proc. SPIE* **8935**, 89350S (2014).
13. T. C. Wood and D. S. Elson, "Polarization response measurement and simulation of rigid endoscopes," *Biomed. Opt. Express* **1**(2), 463–470 (2010).
14. J. Wolfe and R. A. Chipman, "Reducing symmetric polarization aberrations in a lens by annealing," *Opt. Express* **12**(15), 3443–3451 (2004).
15. L. Fu and M. Gu, "Fibre-optic nonlinear optical microscopy and endoscopy," *J. Microsc.* **226**(3), 195–206 (2007).
16. D. C. Leiner, "Miniature optics in the hospital operating room," *Proc. SPIE* **935**, 52–62 (1988).
17. D. M. Huland et al., "*In vivo* imaging of unstained tissues using long gradient index lens multiphoton endoscopic systems," *Biomed. Opt. Express* **3**(5), 1077–1085 (2012).
18. P. Rol et al., "Optical properties of miniaturized endoscopes for ophthalmic use," *Opt. Eng.* **34**(7), 2070–2077 (1995)..
19. X. Li and W. Yu, "Deep tissue microscopic imaging of the kidney with a gradient-index lens system," *Opt. Commun.* **281**(6), 1833–1840 (2008).
20. P. Kim et al., "*In vivo* wide-area cellular imaging by side-view endomicroscopy," *Nat. Methods* **7**(4), 303–307 (2010).
21. J. C. Jung et al., "*In vivo* mammalian brain imaging using one- and two-photon fluorescence microendoscopy," *J. Neurophysiol.* **92**(5), 3121–3133 (2004).
22. W. Su and J. A. Gilbert, "Birefringent properties of diametrically loaded gradient-index lenses," *Appl. Opt.* **35**(24), 4772–4781 (1996).
23. J. Chang et al., "Single-shot spatially modulated Stokes polarimeter based on a GRIN lens," *Opt. Lett.* **39**(9), 2656–2659 (2014).
24. P. S. Hauge, "Mueller matrix ellipsometry with imperfect compensators," *J. Opt. Soc. Am.* **68**(11), 1519–1528 (1978).
25. D. H. Goldstein and R. A. Chipman, "Error analysis of a Mueller matrix polarimeter," *J. Opt. Soc. Am. A* **7**(4), 693–700 (1990).
26. S. Y. Lu and R. A. Chipman, "Interpretation of Mueller matrices based on polar decomposition," *J. Opt. Soc. Am. A* **13**(5), 1106–1113 (1996).
27. H. He et al., "Two-dimensional and surface backscattering Mueller matrices of anisotropic sphere-cylinder scattering media: a quantitative study of influence from fibrous scatterers," *J. Biomed. Opt.* **18**(4), 046002 (2013).
28. A. Ambirajan and D. C. Look, "Optimum angles for a polarimeter: part I," *Opt. Eng.* **34**(6), 1651–1655 (1995).

Biographies of the authors are not available.